Journal of Materials Chemistry B

Preparation and characterization of novel water-based biodegradable polyurethane nanoparticles encapsulating superparamagnetic iron oxide and hydrophobic drug

Journal:	*Journal of Materials Chemistry B*
Manuscript ID:	TB-ART-01-2014-000069.R1
Article Type:	Paper
Date Submitted by the Author:	03-Apr-2014
Complete List of Authors:	Chen, Yen-Ping; Institute of Polymer Science and Engineering, National Taiwan University, Hsu, Shan-hui; Institute of Polymer Science and Engineering, National Taiwan University,

Journal Name Journal of Materials Chemistry B Dynamic Article Links ►

Cite this: DOI: 10.1039/c0xx00000x

www.rsc.org/xxxxxx

ARTICLE TYPE

Preparation and characterization of novel water-based biodegradable polyurethane nanoparticles encapsulating superparamagnetic iron oxide and hydrophobic drug

Yen-Ping Chen and Shan-hui Hsu*

Received (in XXX, XXX) Xth XXXXXXXXX 20XX, Accepted Xth XXXXXXXXX 20XX
DOI: 10.1039/b000000x

Superparamagnetic iron oxide nanoparticles (SPIO NPs) are widely used in magnetic resonance imaging and magnetic hyperthermia. In this study, we used the self-assembly behavior of biodegradable polyurethane nanoparticles (PU NPs) in water to encapsulate SPIO NPs (SPIO-PU NPs) or hydrophobic model drugs (drug-PU NPs) by an in-situ method. PU NPs and SPIO-PU NPs were characterized by the dynamic light scattering (DLS), transmission electron microscopy (TEM), infrared spectroscopy (IR), and thermogravimetric analysis (TGA). The superparamagnetic property and magnetic heating ability of SPIO-PU NPs were assessed. PU NPs had no significant cytotoxicity and could be taken up by cells. SPIO-PU NPs were highly efficient in labeling cancer cells with cellular uptake of ~16 pg iron per cell in average. Hydrophobic drugs were entrapped in PU NPs effectively and showed a sustained release profile. Upon heating, the release of drug was accelerated. This proof-of-concept study demonstrated a novel way to encapsulate SPIO and hydrophobic drug in PU NPs with smart designs for potential applications in cancer diagnostics, hyperthermia, and chemotherapy.

Introduction

Nanoparticles (NPs) are one of the most potential materials in the biomedical field, because they possess unique features in optical, electrical, thermal, and magnetic properties.[1] Some NPs are made from the precious metal and more expensive in cost, for example, gold, silver, or quantum dots. Superparamagnetic iron oxide NPs (SPIO NPs) have relatively low cost and advantages of biocompatibility and biodegradability.[2] SPIO NPs are superparamagnetic innately and attractive tools in several biomedical disciplines, such as magnetic resonance imaging (MRI),[3] hyperthermia treatment,[4] or anti-biofilm.[5] Furthermore, the endothelial cells of cancer tissue have irregular holes due to neovascularization, and NPs can penetrate the cancer tissue through these irregular holes to perform label or medication.[6] Most SPIO NPs, when administered in living body, stay in liver and spleen. Therefore, SPIO NPs can be efficiently used for the treatment of liver cancer.[7] Nanotechnology in cancer therapy is known as a treatment that can potentially combine diagnostics, monitoring of the treatment, and the increase of drug efficacy.[8] Moreover, SPIO NPs are approved for clinical use as an MRI contrast agent by the US Food and Drug Administration (FDA).

SPIO NPs can be synthesized by many methods. Surface modification and the maintenance of the original functionality are important, because the hydrophobic surface leads to precipitation in the aqueous phase.[9] Using a surfactant or mutually exclusive surface charge, or producing a stereoscopic effect, can make SPIO NPs well dispersed in aqueous solution.[10] Sun et al.[11] showed that SPIO NPs modified by the surfactant sodium oleate successfully maintained their superparamagnetic property. SPIO NPs could be further equipped with the ability to carry therapeutic drugs. Many safe biodegradable polymeric materials can entrap drugs, such as poly(lactic-co-glycolic acid) (PLGA) and poly(ε-caprolactone) (PCL).[12] Bae et al.[13] coated a superparamagnetic SPIO NPs with PCL by emulsification. Rutnakornpituk et al.[14] used poly(ethylene glycol) methyl ether (mPEG)-PCL of different molecular weights to coat pre-modified SPIO NPs. The latter work demonstrated that when the hydrophobic PCL segment ratio was increased, the efficiency to carry hydrophobic drugs also increased.

Polyurethane (PU) has good mechanical properties and biocompatibility. The waterborne PU is environment-friendly and sustainable.[15] Waterborne PU has an ionic group to make PU particles dispersed and stored in water.[16] PU water dispersion has low cost as well as low toxicity.[17] It was also possible for PU to stably carry hydrophobic compounds such as anti-cancer drugs. General anti-cancer drugs are hydrophobic, and need a nanocarrier of central core of hydrophobic and biodegradable segment to increase the efficiency of drug delivery. Khosroushahi et al.[18] prepared PU micelles for carrying anti-cancer drugs that rapidly released drugs in response to different pH value. Zhang et al.[19] used triblock PU copolymer to disperse SPIO NPs in water.

However, the procedures to encapsulate drugs often require the use of organic solvent or even toxic chemicals.

In this study, we developed a green procedure to encapsulate SPIO NPs and hydrophobic drugs in biodegradable PU NPs. We used a co-precipitation method to make SPIO NPs (~9 nm), and added to the reaction mixture during the synthesis of novel waterborne biodegradable PU NPs (~40 nm). By the strategy, SPIO NPs could be embedded in PU NPs through the water-dispersible process. We further investigated the physico-chemical properties and cell uptake of these core-shell NPs. Moreover, the hydrophobic model drugs were added in the PU NPs and the drug release behavior was observed. It was expected that the water-based biodegradable PU NPs could serve as a nanoplatform to carry the diagnostic (e.g. SPIO NPs) and therapeutic agents (e.g. drugs) simultaneously for future applications in cancer theranostics.

Materials and methods

Synthesis of SPIO NPs

The synthetic procedure of SPIO NPs was described in a previous study.[22] Iron (II) chloride tetrahydrate (8.95 g) (Alfa Aesar) and iron (III) chloride hexahydrate (18.25 g) (Alfa Aesar) were dissolved in 150 mL distilled water with strong stirring. Subsequently, 11.75 g NaOH (Showa, Japan) was dissolved in 50 mL distilled water and slowly dropped into the precursors and reacted for 30 min at room temperature. When the color of the solution turned into black, SPIO NPs were successfully synthesized as the precipitate. SPIO NPs were washed by centrifugation and redispersion in distilled water for three times. SPIO NPs were then washed again by centrifugation and redispersion in 100% ethanol for several times to remove water.

Synthesis of water-based biodegradable polyurethane nanoparticles (PU NPs)

The preparation procedure of PU NPs is described below. 10 g poly(ε-caprolactone) diol (PCL diol, Mn≈2000 g mol^{-1}, Sigma-Aldrich) and 4.183 g isophorone diisocyanate (IPDI, Evonik Degussa GmbH) were mixed in a 250 mL four-necked flask and reacted for 3 h with mechanical stirring (180 rpm) and under a nitrogen atmosphere at 75°C. After prepolymerization of PCL diol and IPDI, 0.699 g 2,2-bis(hydroxymethyl) propionic acid (DMPA, Sigma-Aldrich) as a chain extender and methyl ethyl ketone (MEK, J.T. Baker) were added to react for 1 h. After that, the temperature was cooled down to 45°C, and 0.505 g triethylamine (TEA, RDH) was added into the reactor to neutralize the carboxylic group of DMPA for 30 min. 36 mL water was quickly added with vigorous stirring (1200 rpm) for 2 min. Subsequently, another chain extender 0.457 g ethylenediamine (EDA, Tedia) in water was added and reacted for 30 min. The residual MEK and TEA were removed by vacuum distillation. The procedures rendered PU NPs in water with a solid content of about 30%. The molar ratio of IPDI/diol/DMPA/TEA/EDA was 1/0.265/0.265/0.265/0.404 for preparing the NPs in water.

Preparations of SPIO-PU NPs and drug-PU NPs

SPIO NPs were washed by centrifugation and redispersion in MEK for several times. SPIO-PU NPs were prepared in situ during polymerization. After mixing TEA in the reactive vessel, SPIO NPs in MEK (~100 mg/mL) were added and mixed with strong stirring (500 rpm) about 50 min. Water was quickly added with vigorous stirring for 2 min. Afterwards, EDA in water was added to complete the polymerization. SPIO-PU NPs successfully dispersed were collected by centrifugation (2500 rpm) and were removed of large aggregates. SPIO-PU NPs were further collected by a magnet where only SPIO-PU NPs were attracted. This method effectively removed blank PU NPs (without SPIO core). The SPIO-PU NPs collected were washed by distilled water. Finally, SPIO-PU NPs were redispersed in distilled water after another magnetic purification. The yield of SPIO-PU NPs was about 45%, which was determined after drying in vacuum by the thermogravimetric method described later. The iron (Fe) concentration of SPIO-PU NPs was determined by the atomic absorption spectroscopy (AA, Thermal Scientific ICE 3000, USA).

Hydrophobic model drug 9-(methylaminomethyl)anthracene (MAMA, Sigma-Aldrich) or anti-cancer drug Vitamin K3 (VK3, Acros Organics) was encapsulated in PU NPs. The drug (50 mg) in MEK (1 mL) was added after mixing TEA in the polymerization step and mixed for 30 sec. Water was quickly added with vigorous stirring for 2 min. Afterwards, EDA in water was added to complete the polymerization. The drug release behavior was later evaluated.

Determination for molecular weight, hydrodynamic size, and zeta potential

The weight average molecular weight of PU was measured by gel permeation chromatography (GPC, Waters Apparatus, USA) in N-methyl-2-pyrrolidone using polystyrene as standards. The apparent molecular weight of each PU NP was determined by the asymmetric flow field flow fractionation (AFFFF, Wyatt) followed by a differential refractometer and multi-angle laser light scattering (MALS).

PU NPs, SPIO-PU NPs, and drug-PU NPs were diluted with distilled water. The diameter and zeta potential of all types of NPs were measured by a submicron particle analyzer (Delsa Nano, Beckman Coulter, USA) which employs dynamic light scattering (DLS) for evaluating diameter and electrophoretic light scattering for evaluating zeta potential.

Transmission electron microscope (TEM)

SPIO NPs and PU NPs were diluted by ethanol and distilled water, respectively. They were dropped onto a carbon-coated copper grid (formvar support films on 200 mesh copper grids, Ladd Research, USA). SPIO-PU NPs were diluted by distilled water and dropped onto a carbon-coated copper grid, and then moved onto a magnet. The magnet allowed SPIO-PU NPs to quickly settle on the grid. After a short period of time (30 sec), the magnet was removed from the grid. After removing the droplets on the grids, all grids were air-dried in room temperature overnight. The samples were examined by TEM (Hitachi H-7100,

75 keV, Japan; JEM-1200EX II, JEOL, 80 keV, Japan). The size was determined by image analysis using a software (ImageJ).

Infrared (IR) spectroscopy

SPIO NPs were dried under vacuum. PU NPs and SPIO-PU NPs were cast and dried under vacuum. SPIO NPs were mixed with KBr for Fourier-Transform IR spectrometry (FTIR, Perkin Elmer, USA) measurement. PU and SPIO-PU films were analyzed by the attenuated total reflection (ATR)-FTIR. The IR spectra were obtained with a resolution of 2 cm^{-1} and 16 scans from 400 cm^{-1} to 4000 cm^{-1}.

Thermal analysis

The thermal stability of dried samples (SPIO NPs and SPIO-PU NPs) was obtained by a thermogravimetric analyzer (TGA Q50, USA) with a heating rate of 10°C min^{-1} from 100°C to 800°C under a nitrogen atmosphere. Through this analysis, the inorganic and organic fractions in the purified SPIO-PU NPs were also determined. Besides, the yield of SPIO encapsulated by PU NPs could be estimated based on the above analysis and the total amount of SPIO added in the reaction mixture.

Magnetic measurement

The magnetic hysteresis (M-H) curve of the resultant SPIO NPs and SPIO-PU NPs were measured at 300 K with a magnetic field between −20 and 20 kOe using a superconducting quantum interference device magnetometer (SQUID, MPMS-7, Quantum Design, USA).

Cytotoxicity studies and the cellular uptake test of NPs

Human hepatoma cells (HepG2) were cultured in Dulbecco's modified Eagle medium-high glucose (DMEM-HG) supplemented with 10% fetal bovine serum (FBS) in a 37°C/5% CO_2 incubator. Cells were seeded at a density of 1×10^4 cells/well in a 96 well culture plate and incubated for 12 h in the incubator. Cells were treated with culture medium containing PU NPs or MAMA-PU NPs at different concentrations (0–1000 μg/mL) and incubated for another 24 h. Cells were then washed with phosphate buffered saline (PBS) for 3–5 times to remove free NPs. The uptake of MAMA-PU NPs was examined by a confocal microscope (BD Pathway™ 435, Bioimaging System, BD Biosciences). Cytotoxicity of PU NPs was further determined by 3-(4,5-dimethyl-thiazol-2-yl)-2,5-diphenyltetrazolium bromide (MTT) assay. MTT solution (0.5 mg/mL, 1×PBS, 75 μL) was added to each well and incubated for 4 h. After the supernatant was removed, dimethyl sulfoxide (150 μL) was added to dissolve the formazan crystals. The absorbance of each well was measured at 550 nm by a multi-mode plate reader (SpectraMax® M5, USA) in the UV-vis mode. The uptake of MAMA-PU NPs by cells was quantified by the plate reader in the fluorescence mode (excitation 260 nm and emission 416 nm).

For the uptake of SPIO-PU NPs, HepG2 cells were seeded at a density of 5×10^4 cells/well in a 24-well culture plate and cultured for 24 h. The culture medium was replaced with that containing different concentrations of SPIO-PU NPs and incubated for another 12 h. Cells were then washed with PBS for 3–5 times to remove free NPs. Cytotoxicity of SPIO-PU NPs was determined by the MTT assay. For the cellular uptake of SPIO-PU NPs, the treatment containing only culture medium (0 μg Fe/mL) and the treatment with PU NPs (200 μg PU/mL, no SPIO) were used as the negative control. Prussian blue staining was used to identify the presence of SPIO.[22] For staining, cells were fixed by 2.5% glutaraldehyde solution for 15 min, washed with PBS, and the Prussian blue agent was added for 1 h before further wash in PBS. The stained cells were observed by an inverted microscope (Leica DMIRB, Germany). To quantify the amount of cellular uptake, the groups of HepG2 cells (with 0 or 25 μg Fe/mL) were washed 3–5 times with PBS to remove the free NPs, detached with 0.25% trypsin, and collected by centrifugation. The cell pellets were dissolved in 20% HNO_3 and diluted to contain 1.5% HNO_3. The iron concentration was quantified by an inductively coupled plasma optical emission spectrometer (ICP-OES, Optima 8300, Perkin Elmer, USA).

Drug release behavior

MAMA and VK3 were the hydrophobic model drug and anti-cancer drug selected as mentioned. All drug-PU NPs were diluted into a suitable solid content using distilled water or sodium chloride solution. The drug release behavior was investigated in different environments including distilled water at 37°C (pH~8.4), distilled water at 50°C (pH~8.4), 0.9% sodium chloride solution at 37°C (pH~8.4), phosphate buffered saline (PBS, pH~7.4) at 37°C, and distilled water at 70°C (pH~8.4), and. After a certain period of time, the release medium of MAMA-PU NPs were collected by centrifugation (5000 rpm) in a centrifugal ultrafilter (3 kDa MWCO, Pall Corporation, USA), and the release medium of VK3-PU NPs were collected with another centrifugal ultrafilter (50 kDa MWCO, Millipore, USA). The optical absorption of release medium in the lower tube was detected by the multi-mode plate reader at 385 nm (MAMA) and 340 nm (VK3). According to a premeasured calibration curve of absorbance vs. drug (MAMA or VK3) concentration, the drug concentration in the release medium was obtained. The drug entrapment efficiency (DEE%) was defined as the amount of encapsulated drug divided by the total drug added. The amount of encapsulated drug was determined by subtracting the initial amount of drug in water from the total drug. The percentage of released drugs was calculated based on the ratio of drug released at each time and the initial drug encapsulated.

Heating tests by an oscillating magnetic field

A high frequency oscillating magnetic field (LT-15-80, Taiwan) was used to heat the dispersions of SPIO NPs and SPIO-PU NPs each containing 1 wt% SPIO NPs. The dispersions in glass tubes were placed near the coil, and an alcohol thermometer was used to measure the temperature of the dispersions. The coil was water-cooled with an auto pumping system. The five-turn coil (0.021 m inner diameter) generated a magnetic field of 20 kA m^{-1}. The temperature was recorded per minute during the exposure to the magnetic field for a period of 15 min. The drug release behavior of SPIO-VK3-PU NPs (where SPIO NPs and VK3 were both encapsulated in PU NPs) was also examined after magnetic

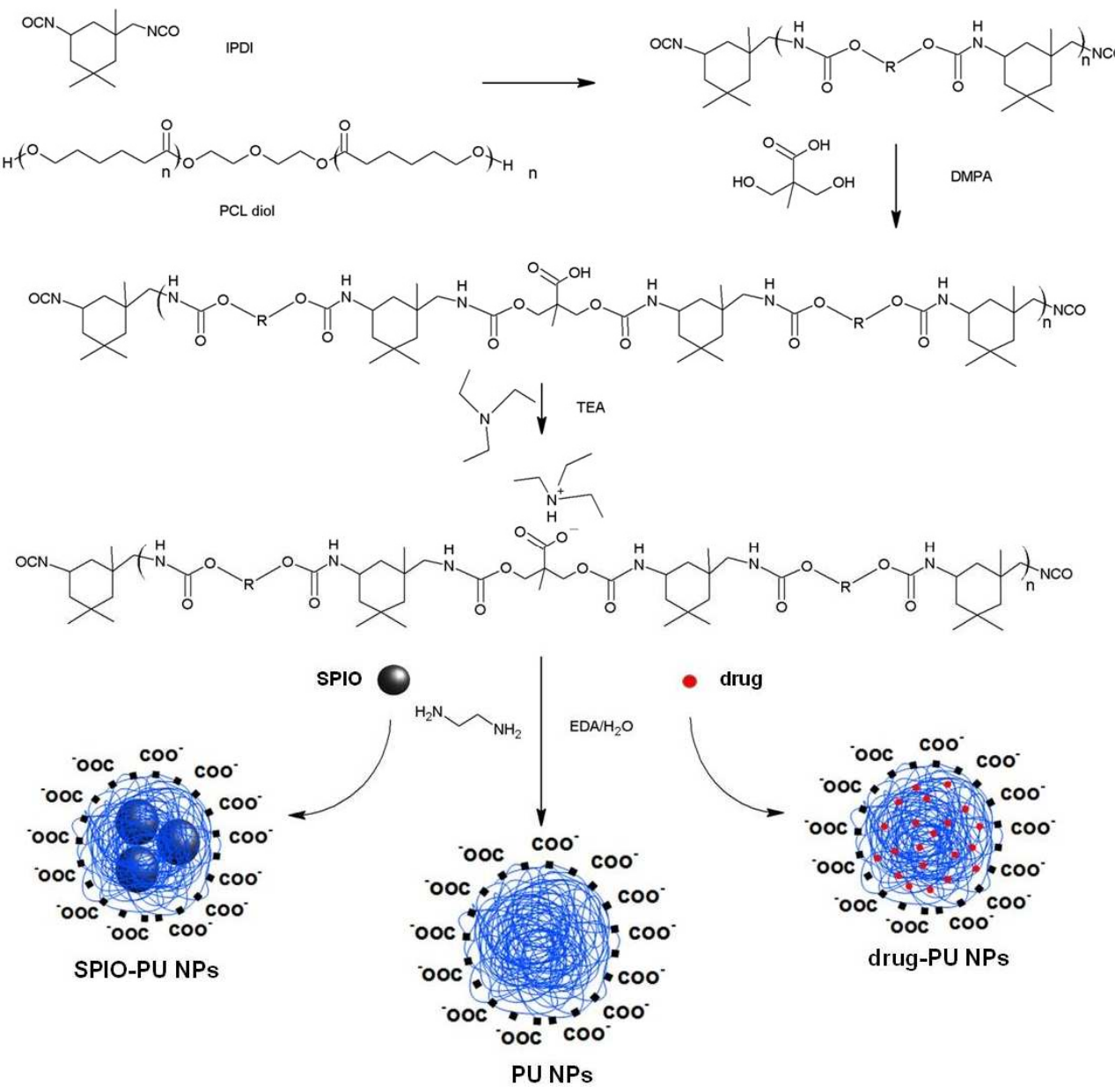

Fig. 1 Schematics for the preparation procedures of PU NPs, SPIO-PU NPs, and drug-PU NPs in this study.

heating with an oscillating magnetic field of 20 kA m^{-1} for 20 min. The release medium after the short-term heating was collected with a 50 kDa centrifugal ultrafilter for detection.

Statistical analysis

The results were expressed as mean ± standard deviation (SD). Statistical differences were analyzed by student's t-test. Data were considered statistically significant when p value is <0.05.

Results

Preparations of various NPs

Bare SPIO NPs were first prepared by co-precipitation. Various PU-based NPs (PU NPs, SPIO-PU NPs, and drug-PU NPs) were prepared during the polymerization process as shown in Fig. 1. PU synthesized had a molecular weight about 165 kDa for single chain and an apparent molecular weight about 6.6×10^4 kDa for each PU NP. The diameter and zeta potential of various NPs determined by light scattering is shown in Table 1. PU NPs had a hydrodynamic diameter of 39.6 ± 4.8 nm and a zeta potential of

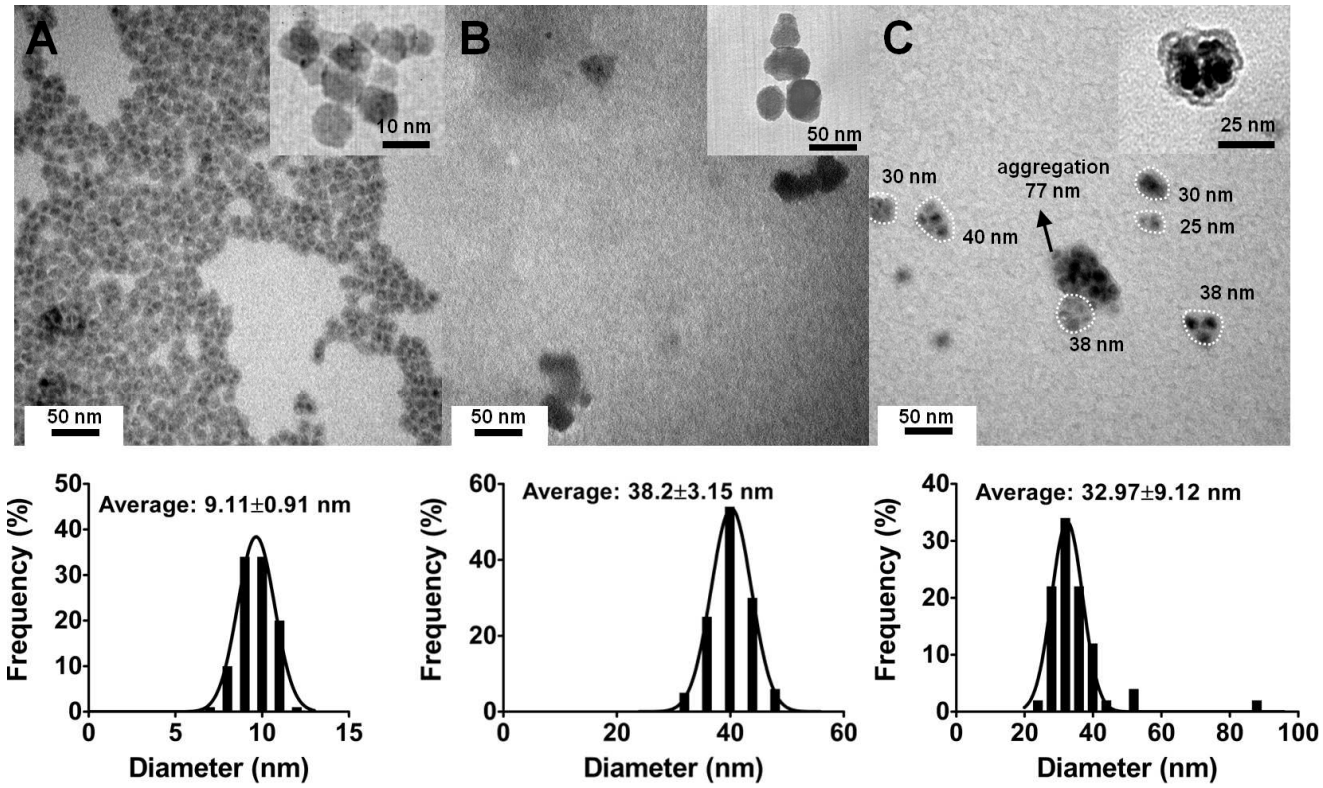

Fig. 2 TEM images and the respective size distribution for (A) SPIO NPs, (B) PU NPs, and (C) SPIO-PU NPs.

−55.3 ± 2.4 mV. SPIO-PU NPs had a smaller hydrodynamic diameter (32.8 ± 1.7 nm) and a less negative zeta potential (−46.7 ± 1.1 mV). Drug-PU NPs, i.e. MAMA-PU NPs and VK3-PU NPs, had hydrodynamic diameters (~32−34 nm) and zeta potentials (~47−49 mV) similar to each other and to SPIO-PU NPs.

Table 1 The hydrodynamic diameter and zeta potential of various NPs prepared in the study.

Samples	Hydrodynamic diameter (nm)	Zeta potential (mV)
PU NPs	39.6 ± 4.8	−55.3 ± 2.4
SPIO-PU NPs	32.8 ± 1.7	−46.7 ± 1.1
MAMA-PU NPs	32.4 ± 1.7	−49.2 ± 2.0
VK3-PU NPs	34.0 ± 3.1	−47.5 ± 2.2

TEM characterization of SPIO-PU NPs

Fig. 2 shows the TEM images and the respective size distribution for SPIO NPs (bare), PU NPs, and SPIO-PU NPs. SPIO NPs prepared by co-precipitation were in round shape with an average diameter of 9.11 ± 0.91 nm. PU NPs were in oval shape with an average diameter of 38.2 ± 3.15 nm. SPIO-PU NPs were somewhat irregular in shape with an average diameter of 32.97 ± 9.12 nm. Each SPIO-PU NPs contained several SPIO NPs in the core. A few aggregates were observed in the image of SPIO-PU NPs.

Characterization by IR spectroscopy

IR spectra for the NPs are shown in Fig. 3A. In the spectrum of SPIO NPs, the absorption peak observed peak at 551 cm^{-1} was

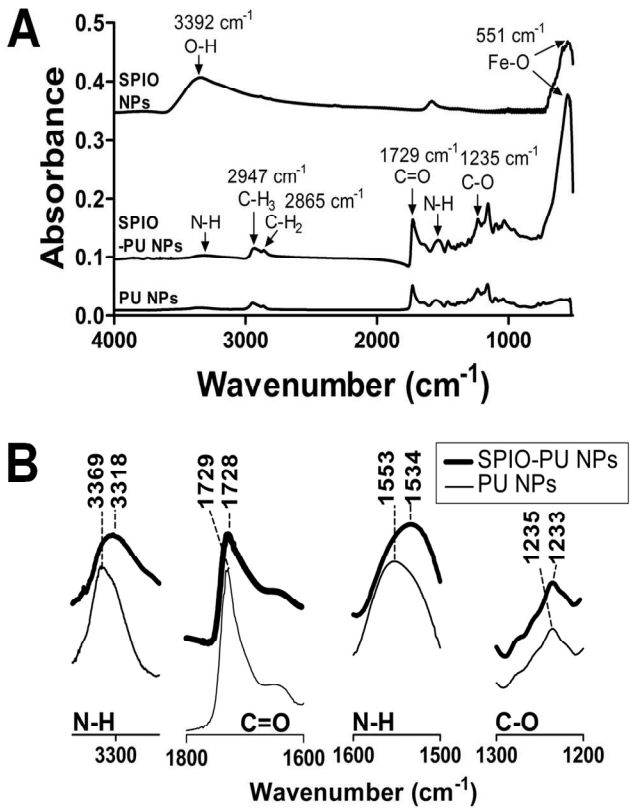

Fig. 3 (A) IR spectra of SPIO NPs, SPIO-PU NPs, and PU NPs. (B) Enlarged IR peaks revealing the changes in certain functional groups of SPIO-PU NPs and PU NPs.

attributed to the vibration of Fe-O bond. Another peak at 3392 cm^{-1} was attributed to the vibration of O-H. In the spectra of PU NPs and SPIO-PU NPs, the peaks at 2947 cm^{-1} and 2865 cm^{-1} were attributed to the C-H_3 and C-H_2 stretching vibrations in the structure of PU. For PU NPs, the broad absorption bands at 3369 cm^{-1} and 1553 cm^{-1} were attributed to the N-H stretching and bending. The peaks at 1729 cm^{-1} and 1235 cm^{-1} were assigned to the vibration of C=O and C-O. For SPIO-PU NPs, the spectrum appeared to be a combination of those of PU NPs and SPIO NPs. As shown in Fig. 3B, the peaks at 3369 cm^{-1} for PU NPs was significantly shifted to 3318 cm^{-1} in SPIO-PU NPs, and that of 1553 cm^{-1} was significantly shifted to 1534 cm^{-1}. On the other hand, peak positions at 1729 cm^{-1} and 1235 cm^{-1} did not change significantly after SPIO encapsulation.

Thermal analysis

The TGA thermograms for various NPs are shown in Fig. 4A. The weight loss and retention were 51.99% and 48.01% for SPIO-PU NPs, each indicating the organic (PU) and inorganic (SPIO) fractions of the NPs. Moreover, the pyrolytic temperature (T_{onset}) and 50% thermal degradation temperature (T_d) of PU were modified in the presence of SPIO NPs. The value of T_{onset} increased from 247°C to 260°C and that of T_d decreased from 247°C to 260°C in SPIO-PU NPs. Furthermore, a second weight loss of SPIO-PU NPs was observed in the high-temperature region (600–700°C) while no weight loss was observed for PU NPs in this region.

Magnetic measurement

The magnetic behavior of prepared SPIO NPs and SPIO-PU NPs measured by SQUID at room temperature is shown in Fig. 4B.

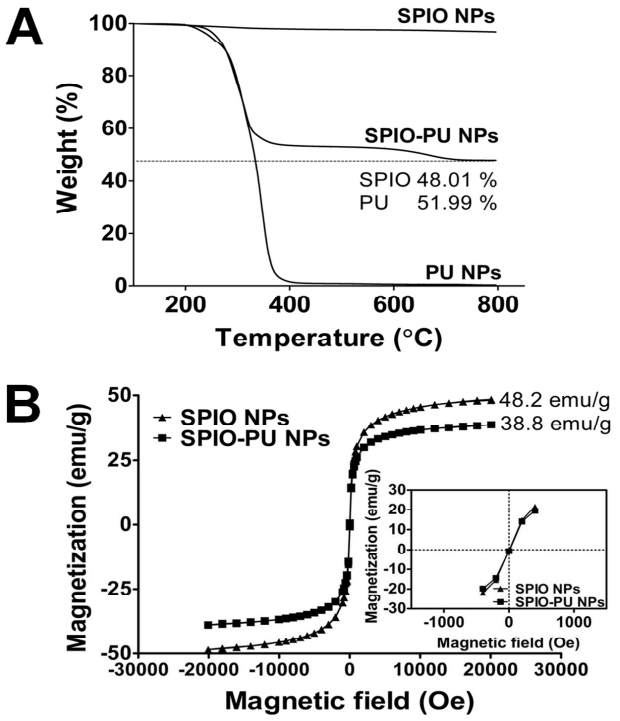

Fig. 4 (A) TGA thermograms for SPIO NPs, SPIO-PU NPs, and PU NPs. (B) The magnetic hysteresis curves of SPIO NPs and SPIO-PU NPs analyzed by SQUID. The inset shows the enlarged curves in the range of +400 and –400 Oe.

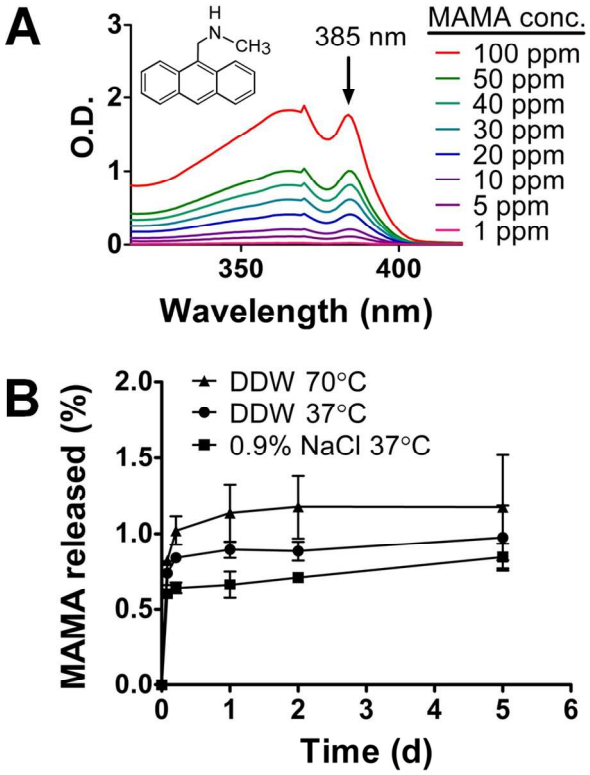

Fig. 5 (A) The UV absorption bands of MAMA at different concentrations. The inset displays the MAMA structure. (B) The drug release behavior of MAMA-PU NPs in different conditions, including water at 37°C, 0.9% NaCl solution at 37°C, and water at 70°C.

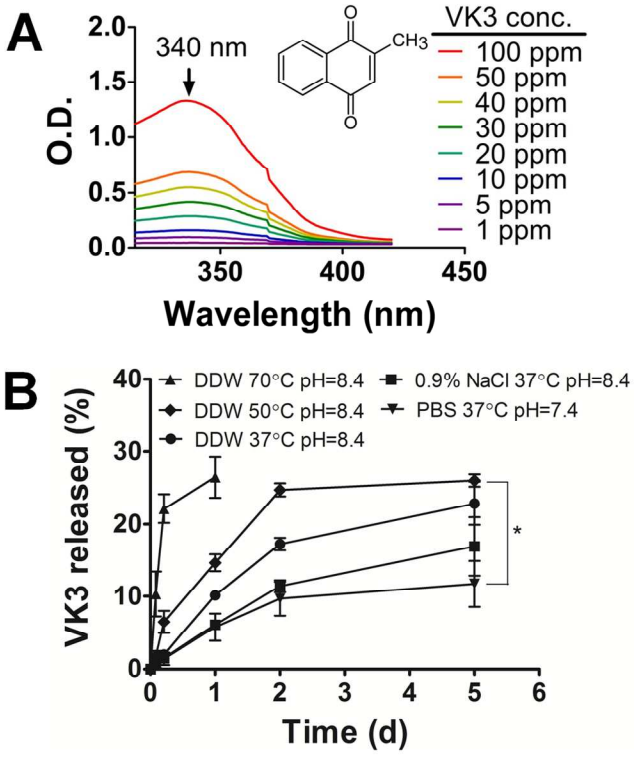

Fig. 6 (A) The UV absorption bands of VK3 at different concentrations. The inset depicts the VK3 structure. (B) The drug released behaviors of VK3-PU NPs in different conditions, including PBS solution (pH~7.4) at 37°C, water (pH~8.4) at 37°C, 0.9% NaCl solution (pH~8.4) at 37°C, water (pH~8.4) at 50°C, and water (pH~8.4) at 70°C.

The saturation magnetization value of SPIO-PU NPs was 38.8 emu g^{-1}, which was a little lower than that of SPIO NPs (48.2 emu g^{-1}). An enlarged portion of the curves (inset) indicated no hysteretic effect. There confirmed that the superparamagnetic property of SPIO NPs was mostly retained after encapsulation in PU NPs.

Drug release profiles

MAMA and VK3 are both hydrophobic compounds. Their UV absorption bands are located in 385 nm (MAMA) and 340 nm (VK3), as shown in Fig. 5A and Fig. 6A. The optical density was used to determine their concentration in the medium. Based on the amount of entrapped drug and the loaded amount, the DEE% value of MAMA-PU NPs was calculated to be 99.24 ± 0.09%. The DEE% value of VK3-PU NPs was 97.01 ± 0.19 %. The drug loading content of both drug-PU NPs in this case was about 0.33% (50 mg drug / 15.31 g PU NPs).

The percent release of MAMA and VK3 from the drug-NPs in different conditions is shown in Fig. 5B and Fig. 6B. MAMA-PU NPs displayed a very slow release (~0.5–1.5%) of MAMA in all conditions within 5 days. The release of VK3 from VK3-PU NPs depended on the conditions. The release of VK3 in PBS (37°C) was ~12% within 5 days, which was the slowest, followed by the release (~17%) in 0.9% NaCl solution for 5 days. As the temperature increased, the release was enhanced. At 37°C and 50°C, there was about ~23% and ~26% of VK3 released from the NPs after 5 days. Moreover, there was about ~26.5% of VK3 released at 70°C after 1 day. No burst release was observed in each condition. The release profiles of VK3 showed two distinct phases with different slopes, i.e. the greater release in 2 days and the smaller release between 2 and 5 days, in particular for the release measured at 50°C.

Cytotoxicity and cellular uptake of PU NPs

The cytotoxicity of PU NPs and MAMA-PU NPs at different concentrations is shown in Fig. 7A. There was no cytotoxic effect at higher concentrations (1000 μg PU/mL) of PU NPs and MAMA-PU NPs. On the other hand, MAMA happened to have weak blue fluorescence. This suggested that MAMA-PU NPs may be a fluorescent tracker for NP uptake. The fluorescent images of HepG2 cells treated with MAMA-PU NPs at 250–1000 μg PU/mL and the quantitative uptake of MAMA-PU NPs are shown in Fig. 7B and Fig. 7C. Although HepG2 also demonstrated slight autofluorescence, those treated with MAMA-PU NPs (in particular at higher concentrations) demonstrated significantly brighter blue fluorescence when compared with the negative control (0 μg PU/mL). These results suggested that PU NPs may be taken up by HepG2. The amount of uptake increased with the concentration of PU NPs.

Cytotoxicity and cellular uptake of SPIO-PU NPs

The cytotoxicity of SPIO-PU NPs with different concentrations of SPIO (0–200 μg Fe/mL) is shown in Fig. 8A. No cytotoxicity was found when cells were exposed to low concentrations (25–50 μg Fe/mL) of SPIO-PU NPs. For concentrations beyond 100 μg Fe/mL, SPIO-PU NPs showed significant cytotoxicity. Prussian blue staining for the endocytosed SPIO-PU NPs is shown in Fig. 8B. The uptake of SPIO-PU NPs was evident even at a low SPIO concentration (10 μg Fe/mL). As the concentration increased, the amounts of cellular uptake were significantly enhanced. No change in cell morphology was observed when the SPIO concentration was below 75 μg Fe/mL. Beyond 100 μg Fe/mL, cells started to have an irregular shape, as shown in Fig. 8B (f). The cellular uptake of SPIO-PU NPs quantified by ICP-OES is shown in Fig. 8C. The amount of uptake by HepG2 cells exposed to 25 μg Fe/mL was ~16 pg Fe per cell, which was much greater than that of the blank group (~1 pg Fe per cell).

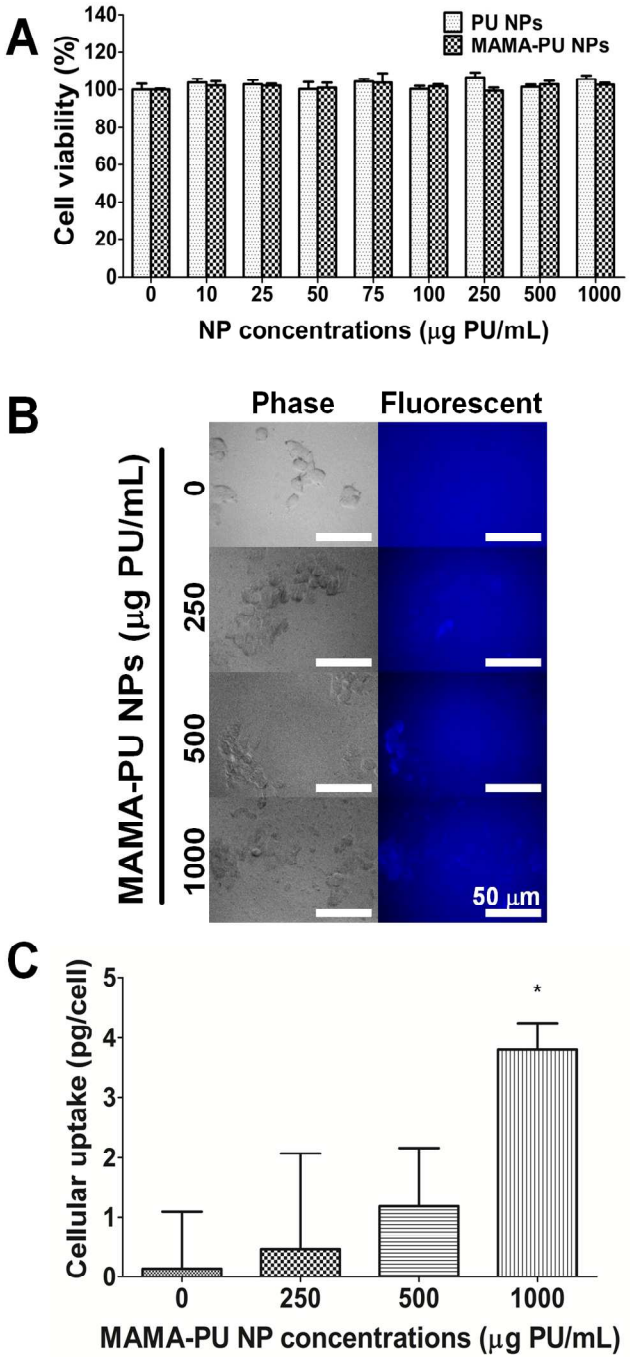

Fig. 7 (A) The viability of HepG2 after incubation with the culture medium containing different concentrations of PU NPs or MAMA-PU NPs. *p < 0.05 with respect to 0 μg PU/mL. (B) Confocal microscopic images showing the uptake of MAMA-PU NPs by HepG2 cells. Scale bar = 50 μm. (C) The amount of uptake of MAMA-PU NPs by HepG2 cells. *p < 0.05 with respect to 0 μg PU/mL.

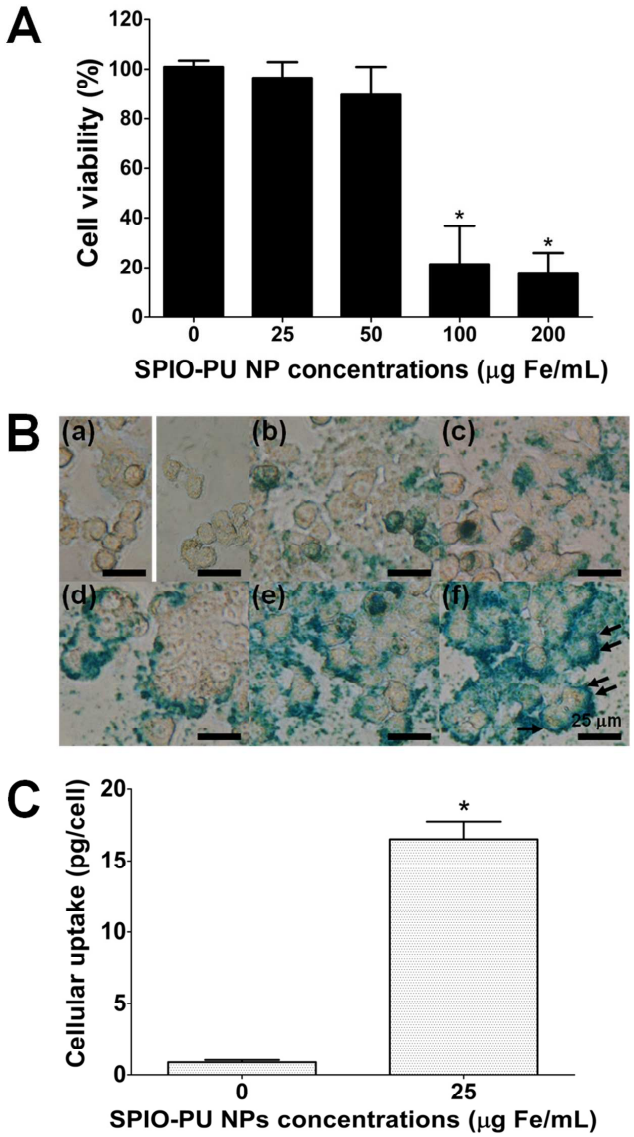

Fig. 8 (A) The viability of HepG2 after incubation with the culture medium containing different concentrations of SPIO-PU NPs. *$p < 0.05$ with respect to 0 μg iron (Fe)/mL. (B) Phase contrast images showing the cellular uptake of SPIO-PU NPs. Images in (a) represent NPs negative control 0 μg Fe/mL (left) and 200 μg PU/mL (right). Images in (b–f) represent 10 (b), 25 (c), 50 (d), 75 (e), and 100 (f) μg Fe/mL, respectively. Cells were stained by Prussian blue staining. Scale bar = 25 μm. Black arrows indicate cells in irregular shapes. (C) The amount of Fe per cell for HepG2 exposed to SPIO-PU NPs [0 (control) or 25 μg Fe/mL], quantified by ICP-OES.

Temperature elevation for SPIO-PU NPs in an oscillating magnetic field

The appearances of SPIO NPs and SPIO-PU NPs before (0 min) and after (15 min) exposure to an oscillating magnetic field (~20 A/m) are shown in Fig. 9A. Bare (uncoated) SPIO NPs began to aggregate and were precipitated during the treatment. SPIO-PU NPs demonstrated no aggregation in the whole process. The magnetic heating curves of SPIO NPs and SPIO-PU NPs containing 1 wt% SPIO are shown in Fig. 9B. The temperature elevation was slower for dispersions of SPIO-PU NPs vs. SPIO NPs in the first 90 sec. Afterwards, the temperature elevation for SPIO-PU NPs was faster. Eventually, the temperature of SPIO-PU NP dispersions rose to 52.1°C after 15 min, which was higher than that of SPIO NP dispersions (46.16°C).

Based on the above findings, a novel PU-based nanotheranostic platform can be designed as shown in Fig. 9C. After magnetic heating, the release of VK3 in SPIO-VK3-PU NPs could be switched on (~3% release during a period of 20 min) and switched off as shown in Fig. 9D. The drug-SPIO-PU NPs may be effectively taken up by cancer cells to provide imaging modality, hyperthermia, and chemotherapy.

Discussion

A green preparation system to encapsulate hydrophobic nanoparticles or drugs was established in this study. The hydrodynamic diameter and zeta potential of various NPs were confirmed by dynamic light scattering. The size of various NPs was in a range of 30–40 nm. These suggested that PU could self-assemble into NPs in an aqueous condition.[20] After encapsulation, the size of PU NPs decreased instead of increased. Because the hydrodynamic diameters of PU NPs may be decreased by reducing the amount of hard segments,[21] we suggested that the hard segments of our PU NPs may be bound or interact with SPIO NPs and hydrophobic drugs to decrease the NP size. Moreover, DMPA was a part of hard segments that contributed to negative zeta potential on PU NPs. A less negative zeta potential was simultaneously observed after SPIO or drug encapsulation.

The size of SPIO NPs synthesized by the co-precipitation method was in a range of 8–20 nm.[11] PU NPs contained about ~400 molecules and the DLS size was very close to the TEM size, suggesting the tight and compact structure of the NPs. Because of the disparity of electron density between SPIO NPs and PU NPs, SPIO-PU NPs demonstrated a PU shell and several SPIO NPs in the core. Some aggregation of SPIO-PU NPs may have occurred when water was removed during sample preparation. Based on the image, there appeared to be 5–10 SPIO NPs within one PU NP capsule.

Observation of Fe-O bond vibration for SPIO NPs was consistent with the previous work.[22] The vibration of O-H (3392 cm^{-1}) was assigned to OH^- (H_2O molecules) absorbed on SPIO NPs.[11] The N-H bond vibration of PU (3369 cm^{-1}) was shifted significantly to 3318 cm^{-1} after SPIO encapsulation. The peak near 3320 cm^{-1} represented the hydrogen-bonded N-H[23] and the peak near 3370 cm^{-1} consisted of the partially hydrogen-bonded N-H as well as free bonds.[21] Therefore, the shift of N-H stretching peak suggested an increase of bonded N-H in PU after SPIO encapsulation. The increase in bonded N-H may be a result of increased hydrogen bond or the interaction between N-H and SPIO.[24]

The pyrolytic temperature (T_{onset}) and 50% thermal degradation temperature (T_d) of PU were modified after SPIO encapsulation. This was attributed to the thermal stability of SPIO. It was reported that the initial heat could be absorbed by SPIO NPs, and afterwards the thermal degradation process of the coating layer was accelerated by the accumulated heat of SPIO NPs.[25, 26] This may explain why the T_{onset} and T_d values in SPIO-PU NPs were respectively higher and lower than PU NPs. In addition, a second thermal degradation temperature of SPIO-PU NPs was observed, which may be the final thermal degradation for the small portion of PU that interacted with the surface of SPIO NPs. Based on the

weight fraction of SPIO and PU in each NP and the densities of the bulk SPIO (5.18 g cm^{-3} [27]) and PU (1.167 g cm^{-3}), the number of SPIO NPs encapsulated in one PU NP was estimated to be about eight after calculation.

It has been reported that polystyrene encapsulating a plurality (~3–15) of SPIO NPs (15–20 nm) could retain >90% saturation magnetization value of SPIO NPs.[28] In our study, SPIO-PU NPs could retain >80% saturation magnetization value. Moreover, SPIO-PU NPs did not preserve any magnetism after removal of the magnetic field in room temperature, suggesting that SPIO NPs encapsulated in PU NPs remained to be superparamagnetic.[29, 30]

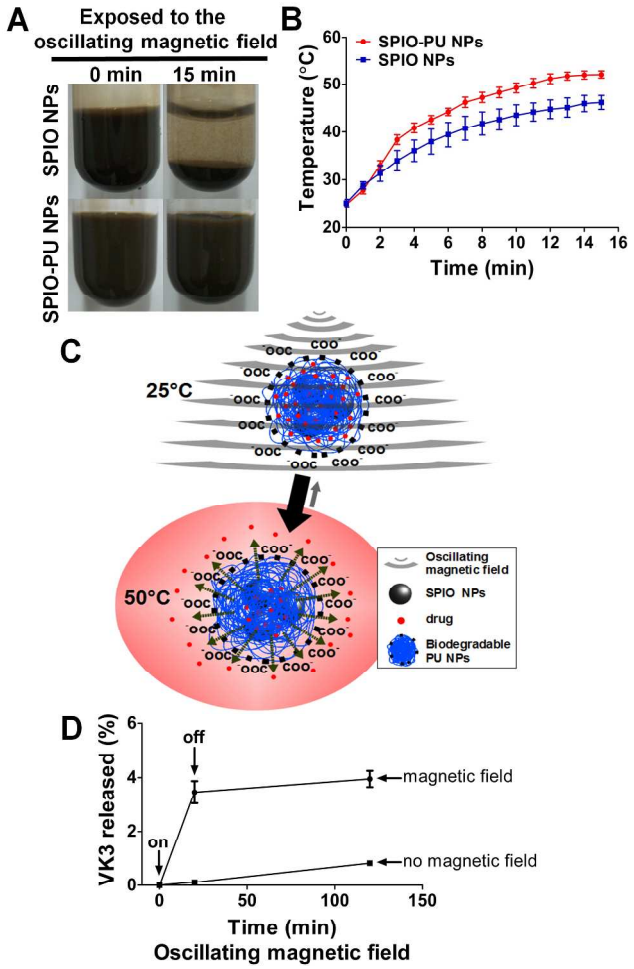

Fig. 9 (A) The appearance of dispersions of SPIO NPs and SPIO-PU NPs before (0 min) and after (15 min) the treatment by an oscillating magnetic field. (B) Magnetic heating curves of SPIO NPs and SPIO-PU NPs containing 1 wt% SPIO NPs exposed to an oscillating magnetic field. (C) Schematics for the design of a novel biodegradable PU NP-based theranostic platform. (D) Fast release of VK3 (switch-on and switch-off) upon magnetic heating.

In order to avoid a strong optical density from PU NPs, centrifugal ultrafiltration[31] was used to separate the release medium from the drug-PU NPs. Literature has reported that the secondary amine of MAMA could be a derivatization reagent which tested the stabilization of the isocyanate (NCO).[32] In the preparation of MAMA-PU NPs, MAMA may react with the isocyanate in both ends of the PU prepolymer to become a drug-polymer conjugate and be chemically encapsulated in PU NPs. Therefore, MAMA displayed a very slow release profile. VK3 did not have functional group to react with isocyanate during encapsulation. The hydrophobic PCL segment can carry hydrophobic drug efficiently.[20] Therefore, VK3 was physically encapsulated in PU NPs and may not form a chemical conjugate with PU. The release of VK3 from PU NPs was significantly faster than that of MAMA. In spite of very high DEE% (>95%) for both drugs, the value for MAMA-PU NPs was even higher than that for VK3-PU NPs. The slight difference may also be attributed to the chemical vs. physical nature of drug encapsulation. The drug loading content could be further enhanced from 0.33% to 4.83% (0.738 g drug / 15.31 g PU NPs) (Supplementary Table S1 provided in the ESI†). At this high loading, the encapsulation efficiency decreased from ~97% to ~74% but was still reasonable.

As the release behavior of drug was important for cancer chemotherapy, the release profiles of VK3 from PU NPs under different environmental conditions were evaluated. In 0.9% NaCl solution, the release of VK3 was slower than that in distilled water. PBS contained 0.9% NaCl and buffering salts. The condition made NPs even more compact and release less drug. This slower release may be associated with the shrinkage of PU NPs in the strong electrolyte solution (i.e. salting out). The release of VK3 from PU NPs could be further regulated by the temperature. At 50°C, the hydrodynamic diameter of the compact PU NPs increased from ~39 nm to ~45 nm (Supplementary Fig. S1 provided in the ESI†), which led to a ~45% increase in volume. At 70°C, the hydrodynamic diameter and volume change of PU NPs were even greater. The temperature-responsive change in hydrodynamic diameter was reversible upon heating and cooling. Literature has reported that drug encapsulated in PEG-PCL micelles could be released more readily when the temperature exceeded the melting temperature of PCL segment.[33] The softening point of our PCL diol (provided by the manufacturer) was 50–60°C. This may explain the hydrodynamic diameter increase of the NPs and more VK3 release from the NPs observed at temperatures beyond 50°C. It has been proposed that if 60–70% of the drug was released from the carrier in a short period (burst release), it was ascribed to the fraction that was loosely adsorbed on the surface of the carrier.[34] Drug-PU NPs in this study revealed no burst release, suggesting that drug was uniformly dispersed in the NPs and may rely on diffusion to be released. On the other hand, MAMA-PU NPs displayed some burst release. We hypothesized that the first phase of release (fast release) within 2 days may be associated with the drug at the outer layer of NPs. The second phase of release (slow release) between 2 and 5 days may be attributed to the diffusion of drug from the tight and compact inner core of PU NPs. VK3 has been reported to treat pancreatic cancer[35] and when combined with vitamin C, has a potential to treat the prostate cancer.[36, 37] The cytotoxicity data in Supplementary Fig. S2 (in the ESI†) showed that VK3-PU NPs did not cause a cytotoxic effect to HepG2. This study used the hydrophobic model drug (MAMA and VK3) to assess the encapsulation efficiency and drug release capability of PU NPs. In literature, the general anti-cancer drugs paclitaxel (PTX) or doxorubicin (DOX) were often encapsulated by in micelles of block copolymers.[38] The advantage of our system is the high DEE% and the in-situ green preparation of drug-NPs.

However, the possible reaction between anti-cancer drugs during NP preparation should be considered. If chemical reactions do occur, the molar ratio of isocyanate group to encapsulate the anti-cancer drugs has to be adjusted for obtaining a satisfactory release profile. In addition, the degradation profile measured at 50°C for PU bulk films revealed slow degradation (<5%) in a week and slight degradation (~12%) after two weeks (Supplementary Fig. S3 provided in the ESI†). The PCL-based PU in this study can undergo biodegradation.[39] We suggested that the drug release from NPs may enter another phase after NP degradation. Moreover, the degradation rate of PU can be designed to give a proper drug release profile.

Non-biodegradable anionic PU NPs have been reported to have low cytotoxicity[17] and good blood compatibility.[40] The cytotoxcity of PU NPs and MAMA-PU NPs at different concentrations was evaluated in vitro using HepG2 cells. Both NPs at a high concentration of 1000 μg PU/mL did not show any cytotoxicity. MAMA as a model drug did not bring any extra cytotoxicity, because it was slowly released from PU NPs. In addition, MAMA has blue fluorescence which makes MAMA-PU NPs blue fluorescent NPs. MAMA-PU NPs of high concentrations (250–1000μg PU/mL) had no cytotoxicity and cells were observed with blue fluorescence. The latter conveniently confirmed that cells may take up PU NPs. Our finding was consistent with the report that anionic PCL-PEG based PU micelles (<100 nm) could be endocytosed by cancer cells.[41] To better assess the cytotoxicity, a normal healthy cell line (L929 skin fibroblasts) and a lung cancer cell line (A549 adenocarcinomic human alveolar basal epithelial cells) were also tested (Supplementary Fig. S4 provided in the ESI†). No cytotoxicity was observed up to 250 μg PU/mL, though the viability of L929 and A549 decreased at 1000 μg PU/mL. At this high concentration (~1000 μg PU/mL), anionic PU NPs flocculated slightly in the culture medium, which may result from the shrinkage of double layer around the NPs in the presence of salt in the culture medium.[42] This flocculation may be a partial cause for the cytotoxicity.

Based on Supplemental Fig. S5 (provided in the ESI†), SPIO-PU NPs at 100 μg Fe/mL were not cytotoxic to L929 fibroblasts, but showed some toxicity to A594 and HepG2 (cancer cells). The latter two cells (A594 and HepG2) thus seemed to be more susceptible to SPIO-PU NPs. On the other hand, the toxicity of pure SPIO NPs could not be determined because they were not dispersed in water. Nevertheless, the toxicity of surfactant (sodium oleate)-stabilized SPIO NPs also revealed slight cytotoxicity to L929 fibroblasts at 100 μg Fe/mL (Supplementary Fig. S6, provided in the ESI†). Therefore, SPIO-PU NPs were not more cytotoxic than the oleate-SPIO NPs for the normal cell line.

Images of Prussian blue staining showed that the HepG2 cells treated with lower concentrations (0–75 μg Fe/mL) of SPIO-PU NPs had a normal shape and good cell attachment to TCPS, while those treated with SPIO-PU NPs at higher concentrations of SPIO-PU NPs (e.g. 100 μg Fe/mL) were irregular in cell morphology. SPIO NPs with a concentration of 25 μg Fe/mL are normally used for cell labeling[22] and the uptake is often about 5 pg Fe/cell. Based on the cellular uptake of SPIO-PU NPs quantified in this study (~16 pg Fe/cell), the SPIO-PU NPs developed was very efficiently endocytosed by cancer cells.

SPIO NPs can respond to the oscillating magnetic field that induces heating. This can be considered as mean of hypothermia in cancer therapy. SPIO NPs encapsulated by a PEG-PCL copolymer were reported to have delayed heating within a short time (~2 min) after the treatment by an oscillating magnetic field, because of the heat absorbed by the PCL segment of the copolymer on the particulate surface.[33] The delayed heating of SPIO-PU NPs within a short time (~90 sec) may be attributed to a similar reason. After that, the environment temperature was rapidly heated up in 1–3 min. During the treatment, SPIO-PU NPs remained well dispersed. On the other hand, aggregations of bare SPIO NPs may have limited the magnetic heating ability so the ultimate temperature was lower vs. SPIO-PU NPs. A commercial and clinical MRI agent (Resovist®, SPIO) has been heated to 50–60°C in one minute using a strong magnetic field (33 kA/m) and an optical temperature sensor.[4] Even though we used a different magnetic field and to record by a regular thermometer, the heat conduction of SPIO NPs appeared to be quick enough for detection of temperature rising.

Finally, we proved that SPIO NPs and VK3 could be simultaneously encapsulated in the same PU NPs (Supplementary Fig. S7, provided in the ESI†). Moreover, the drug release of SPIO-VK3-PU NPs could be switched on and off in short term by the magnetic heating of SPIO. Based on this proof-of-concept study, drug-SPIO-PU NPs could be designed to respond to the heat induced by an oscillating magnetic field that further triggers the local drug release from the thermal swelling of PU NPs. In the mean time, drug-SPIO-PU NPs may enter cells efficiently. These smart designs may find theranostic applications as MRI agents or in combining cancer hyperthermia and chemotherapy.

Conclusions

In this study, we developed an in-situ method to conveniently encapsulate the SPIO NPs or hydrophobic drugs by the self-assembly behavior of PU NPs. Each SPIO-PU NPs contained 48 wt% SPIO and the number of SPIO NPs in one capsule was estimated to be eight. Moreover, SPIO-PU NPs retained the functionality of SPIO and may enter cells effectively. Hydrophobic drug (VK3) was encapsulated by PU NPs efficiently and showed a slow release profile. The release of VK3 from PU NPs was accelerated when the temperature was raised to 50°C, which could be reached through magnetic heating. This study showed that the potential of water-based biodegradable PU NPs as smart carriers for SPIO and drug release. They may serve as a theranostic nanoplatform for cancer therapy in the future.

Acknowledgements

This work was supported by the National Research Program for Nanoscience and Nanotechnology sponsored by the National Science Council (101-2120-M-002-002). We are grateful to Professors Ting-Yu Liu and Wen-Yen Chiu for kindly providing the magnetic heating equipment. We are also obliged to the Precious Instrument Center of National Taiwan University and Ms. Chia-Ying Chien and Ms. Ya-Yun Yang for providing the TEM facility and technical assistance.

Notes

Institute of Polymer Science and Engineering, National Taiwan University, Taipei, 10617, Taiwan, R.O.C. E-mail: shhsu@ntu.edu.tw; Fax: +886+2+33665237;Tel: +886+2+33665313

† Electronic Supplementary Information (ESI) available: The high drug loading content, the hydrodynamic diameter changes of PU NPs at high temperature, the cytotoxicity of VK3-PU NPs, the degradation of PU, the cytoxicity of PU NPs and SPIO-PU NPs to other cells, the cytotoxicity of SPIO, and the detection of VK3 in SPIO-drug-PU NPs. See DOI: 10.1039/b000000x/

References

1 F. E. Kruis, H. Fissan and A. Peled, *J. Aerosol Sci.*, 1998, **29**, 511-535.

2 N. Ahmed, H. Fessi and A. Elaissari, *Drug Discov Today*, 2012, **17**, 928-934.

3 E. C. Cho, C. Glaus, J. Chen, M. J. Welch and Y. Xia, *Trends Mol. Med.*, 2010, **16**, 561-573.

4 T. J. Li, C. C. Huang, P. W. Ruan, K. Y. Chuang, K. J. Huang, D. B. Shieh and C. S. Yeh, *Biomaterials* 2013, **34**, 7873-7883.

5 E. N. Taylor and T. J. Webster, *Int. J .Nanomed.*, 2009, **4**, 145-152.

6 E. M. Pridgen, R. Langer and O. C. Farokhzad, *Nanomedicine-UK*, 2007, **2**, 669-680.

7 J. Wang, Y. Chen, B. A. Chen, J. H. Ding, G. H. Xia, C. Gao, J. A. Cheng, N. Jin, Y. Zhou, X. M. Li, M. Tang and X. M. Wang, *Int. J. Nanomed.*, 2010, **5**, 861-866.

8 L. S. Wang, M. C. Chuang and J. A. Ho, *Int. J. Nanomed.*, 2012, **7**, 4679-4695.

9 W. Wu, Q. He and C. Jiang, *Nanoscale Res. Lett.*, 2008, **3**, 397-415.

10 N. T. K. Thanh and L. A. W. Green, *Nano Today*, 2010, **5**, 213-230.

11 J. Sun, S. B. Zhou, P. Hou, Y. Yang, J. Weng, X. H. Li and M. Y. Li, *J. Biomed. Mater. Res. A*, 2007, **2**, 333-341.

12 R. Gref, Y. Minamitake, M. T. Peracchia, V. Trubetskoy, V. Torchilin and R. Langer, *Science*, 1994, **263**, 1600-1603.

13 S. J. Bae, J. A. Park, J. J. Lee, G. H. Lee, T. J. Kim, D. S. Yoo and Y. M. Chang, *Curr. Appl. Phys.*, 2009, **9**, 19-21.

14 M. Rutnakornpituk, S. Meerod, B. Boontha and U. Wichai, *Polymer*, 2009, **50**, 3508-3515.

15 K. L. Noble, *Prog. Org. Coat.*, 1997, **32**, 131-136.

16 O. Jaudouin, J. J. Robin, J. M. Lopez-Cuesta, D. Perrin and C. Imbert, *Polym. Int.*, 2012, **61**, 495-510.

17 Q. S. Zhu, Y. Wang, M. Zhou, C. Mao, X. H. Huang, J. C. Bao and J. Shen, *J. Nanosci. Nanotechnol.*, 2012, **12**, 4051-4056.

18 A. Y. Khosroushahi, H. Naderi-Manesh, H. Yeganeh, J. Barar and Y. Omidi, *J. Nanobiotechnology*, 2012, **10**, DOI: 10.1186/1477-3155-10-2.

19 Q. A. Zhang, M. S. Thompson, A. Y. Carmichael-Baranauskas, B. L. Caba, M. A. Zalich, Y. N. Lin, O. T. Mefford, R. M. Davis and J. S. Riffle, *Langmuir*, 2007, **23**, 6927-6936.

20 M. M. Ding, J. H. Li, H. Tan and Q. Fu, *Soft Matter*, 2012, **8**, 5414-5428.

21 S. B. Zhang, H. T. Lv, H. Zhang, B. Wang and Y. M. Xu, *J. Appl. Polym. Sci.*, 2005, **101**, 597-602.

22 S. H. Hsu, T. T. Ho and T. C. Tseng, *Biomaterials*, 2012, **33**, 3639-3650.

23 V. W. Srichatrapimuk and S. L. Cooper, *J. Macromol. Sci. Phys.*, 1978, **B15**, 267-311.

24 H. S. Hung, M. Y. Chu, C. H. Lin, C. C. Wu and S. H. Hsu, *J. Biomed. Mater. Res. A*, 2012, **100A**, 26-37.

25 B. Das, M. Mandal, A. Upadhyay, P. Chattopadhyay and N. Karak, *Biomed. Mater.*, 2013, **8**, DOI: 10.1088/1748-6041/8/3/035003.

26 Z. H. Guo, K. Lei, Y. T. Li, H. W. Ng, S. Prikhodko, H. T. Hahn, *Compos. Sci. Technol.*, 2008, **68**, 1513-1520.

27 M. H. Liao and D. H. Chen, *Biotechnol. Lett.*, 2002, **24**, 1913-1917.

28 M. Giardiello, T. O. McDonald, P. Martin, A. Owen and S. P. Rannard, *J. Mater. Chem.*, 2012, **22**, 24744-24752.

29 A. K. Gupta and M. Gupta, *Biomaterials*, 2005, **26**, 3995-4021.

30 R. W. Chantrell, J. Popplewell and S. W. Charles, *IEEE T. Magn.*, 1978, **14**, 975-977.

31 K. S. Soppimath, T. M. Aminabhavi, A. R. Kulkarni and W. E. Rudzinski, *J. Controlled Release*, 2001, **70**, 1-20.

32 P. Tremblay, J. Lesage, C. Ostiguy and H. Van Tra, *Analyst*, 2003, **128**, 142-149.

33 A. L. Glover, J. B. Bennett, J. S. Pritchett, S. M. Nikles, D. E. Nikles, J. A. Nikles and C. S. Brazel, *IEEE T. Magn.*, 2013, **49**, 231-235.

34 M. Fresta, G. Puglisi, G. Giammona, G. Cavallaro, N. Micali and P. M. Furneri, *J. Pharm. Sci.*, 1995, **84**, 895-902.

35 S. Osada, H. Tomita, Y. Tanaka, Y. Tokuyama, H. Tanaka, F. Sakashita and T. Takahashi, *Anticancer Res.*, 2008, **28**, 45-50.

36 B. Tareen, J. L. Summers, J. M. Jamison, D. R. Neal, K. McGuire, L. Gerson and A. Diokno, *Int. J. Med. Sci.*, 2008, **5**, 62-67.

37 J. M. Jamison, J. Gilloteaux, H. S. Taper and J. L. Summers, *J. Nutr.*, 2001, **131**, 158S-160S.

38 N. Rapoport, *Prog. Polym. Sci.*, 2007, **32**, 962-990.

39 Y. Hong, J. Guan, K. L. Fujimoto, R. Hashizume, A. L. Pelinescu and W. R. Wagner, *Biomaterials*, 2010,**31**,4249-4258.

40 C. Mao, L. C. Jiang, W. P. Luo, H. K. Liu, J. C. Bao, X. H. Huang and J. Shen, *Macromolecules*, 2009, **42**, 9366-9368.

41 M. M. Ding, N. J. Song, X. L. He, J. H. Li, L. J. Zhou, H. Tan, Q. Fu and Q. Gu, *ACS Nano*, 2013, 7, 1918-1928.

42 M. Tielemans, P. Roose, P. De Groote and J. C. Vanovervelt, *Prog. Org. Coat.*, 2006, **55**, 128-136

A green and novel in situ encapsulation method for SPIO and hydrophobic drug by PU NPs was developed, where drug release may be accelerated upon magnetic heating.